Supporting Information

All-Colloidal Parity-Time-Symmetric Microfiber Lasers Balanced between the Gain of Colloidal Quantum Wells and the Loss of Colloidal Metal Nanoparticle

*Sina Foroutan-Barenji, Farzan Shabani, Tarik Isik, Zeynep Dikmen, and Hilmi Volkan Demir**

S. F. B., F. S., T. I., Z. D., Prof. H. V. D.
Department of Electrical and Electronics Engineering
Department of Physics
UNAM – Institute of Materials Science and Nanotechnology
Bilkent University
Ankara 06800, Turkey
*E-mail: volkan@bilkent.edu.tr

Z. D.
Faculty of Engineering, Department of Biomedical Engineering
Osmangazi University
Eskisehir 26040, Turkey

Prof. H. V. D.
LUMINOUS! Centre of Excellence for Semiconductor Lighting and Displays
Centre of Optical Fiber Technology
The Photonics Institute
School of Electrical and Electronic Engineering
School of Physical and Mathematical Sciences
School of Materials Science and Engineering
Nanyang Technological University
50 Nanyang Avenue, Singapore 639798, Singapore
*E-mail: hvdemir@ntu.edu.sg

PT symmetry breaking: In the time domain, the interaction between the modes in the gain/loss regions are described by two coupled differential equations for their modal amplitudes:

$$\frac{da}{dt} = -i\omega_a a + i\kappa b + \gamma_a a \quad \text{(S1)}$$

$$\frac{db}{dt} = -i\omega_b b + i\kappa a + \gamma_b b \quad \text{(S2)}$$

where $\gamma_a = g_a - 1/\tau$ and $\gamma_b = g_b - 1/\tau$ are the net gain/loss in each ring. The coupling coefficient κ between the two rings at the radial direction is equivalent to the κ between two parallel waveguides. g_a and g_b are the gain coefficients of the respective resonators. $1/\tau$ represents the intrinsic losses, including scattering, absorption and radiation, which assumed to be equal to both rings. Without coupling, $\omega_a = \omega_b = \omega_0$, when there is coupling, the eigenfrequencies can be obtained by solving the coupled rate equations:

$$\omega^{(a,b)} = \omega_0 + i\frac{\gamma_a + \gamma_b}{2} \pm \sqrt{\kappa^2 - \frac{(\gamma_a - \gamma_b)^2}{2}} \quad \text{(S3)}$$

Here, γ can be defined as the gain-loss contrast between the coupled modes $\gamma = \gamma_a - \gamma_b$. In the PT-symmetric phase, i.e. $\gamma_a = -\gamma_b$, Eq. 2 simplifies to:

$$\omega^{(a,b)} = \omega_0 \pm \sqrt{\kappa^2 - \gamma^2} \quad \text{(S4)}$$

This relation clearly shows that any pair of modes, whose gain/loss remains below the coupling coefficient $\gamma(\omega) < \kappa(\omega)$, will remain neutral. The absence of any overall gain or loss will result in a mode residing equally in the amplifying and lossy regions. On the other hand, as soon as the $\gamma(\omega) > \kappa(\omega)$, PT-symmetry will split into two energy-degenerate lasing/decaying modes.

The Eq. 4 is derived based on the assumption that there is a perfect PT-symmetry in the system, which means both rings should have the exact same resonance frequency, and the same amount of gain/loss. In reality, perfect gain and loss balance never can be reached, considering the inevitable influence of pump distribution inhomogeneities and fabrication imperfections. However, the strong coupling between the ring resonators makes this approach resilient to such perturbations, and the mode suppression capability can be preserved even for deviations from perfect PT symmetry.[1] In a structure with asymmetric gain/loss coefficients, single mode PT-symmetry breaking can be achieved by having $\kappa < |(\gamma_a - \gamma_b)/2|$ for the fundamental mode, while keeping $\kappa > |(\gamma_a - \gamma_b)/2|$ for all other modes. According to Eq. 3, each pair of modes exhibits a common offset $(\gamma_a + \gamma_b)/2$. Hence, to impede any amplification of the higher order modes, the relation $\gamma_b < -\gamma_a$ should be consistent for them. It can be achieved by applying a slight lossy bias to the loss ring to make sure that its attenuation cannot be surpassed by the gain ring's gain.[1,2]

PT arrangement in the radial direction does not suppress the longitudinal WGM modes along the ring. The PT arrangement is preserved in the radial direction and only suppresses high-order transverse modes, just keeping the fundamental mode active. This clearly results in threshold reduction by reducing photon loss to higher-order leaky transverse modes.

The spectral purification is due to the difference between the refractive indices of nanocomposite and CQW films. As shown in Figure 1f in the main text, the refractive index of the nanocomposite and CQW film are not the same at all wavelengths. As a result, the PT-symmetry effect will not be the same for the whole wavelength range of emission.

To further analyze this effect, we model the gain spectrum of the material as a generalized Gaussian function $G(\lambda)=G_c\exp-(|\lambda-\lambda_c|/\alpha)^{\beta}$.[3] The CQW film is our gain medium subject to optical excitation. The saturation gain coefficient at the peak wavelength λ_c=650 nm can be obtained approximately from the notion of negative absorption for the saturated gain medium $G_c=4\pi\kappa/\lambda_c$. From the measured extinction coefficient of κ=0.025 at the peak wavelength, we obtain G_c=5000 cm^{-1}. Here, β and α are related to the shape and width of the distribution, respectively. Using $\kappa=G\lambda/4\pi$ we can calculate the approximate value of κ for the gain medium. Figure R3 depicts the imaginary part of the refractive indices of nanocomposite and calculated κ from the gain spectrum. There is a wavelength (650 nm) at which the gain/loss contrast is enough to break the PT-symmetry $\kappa < |(\gamma_a - \gamma_b)/2|$.

As shown for the case of *f=3.8%*, if the gain/loss contrast is below this critical value, then we will have a smaller gain coefficient due to the losses introduced by the lossy medium; otherwise, in the case of *f=7.1%,* a conjugate pair of lasing and decaying modes emerges, at which the calculated gain coefficient for the fundamental lasing mode from numerical simulations is at the highest. In this case the PT-symmetry arrangement clearly makes the gain profile sharper. As a result, one of the longitudinal modes in the system will have the largest gain and will thus lase before all other modes. These simulation results are consistent with theoretical expectations and experimental observations. It is clear that, in order to obtain this result, some mismatch in the gain/loss system in the emission range of the CQWs is required, dictating loss to be more than gain.[2] Otherwise as shown in Figure S1 for the case of *f =3.8 %*, the Im(β) will be lower and smoother at the peak, resulting in multimode lasing. Figure S2 shows the measurement result in the case of *f=3.8 %* with its threshold higher compared to the case of *f=7.1 %* and lower compared to that of the control sample.

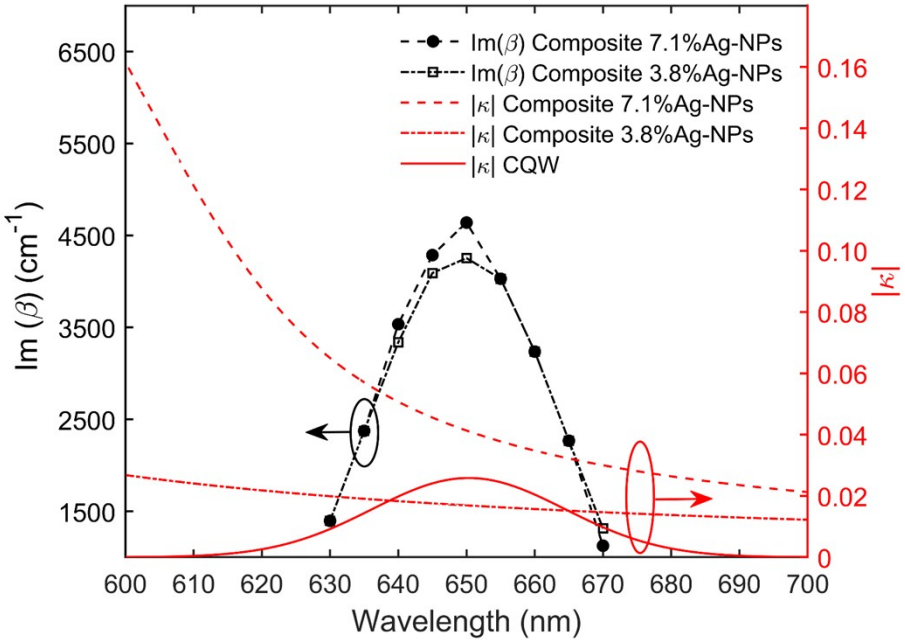

Figure S1. Gain/loss of the AgNPs-PMMA nanocomposite film and the CQW film (shown by dashed and solid lines, respectively) together with imaginary eigenspectral of the fundamental lasing mode in the gain medium (black lines).

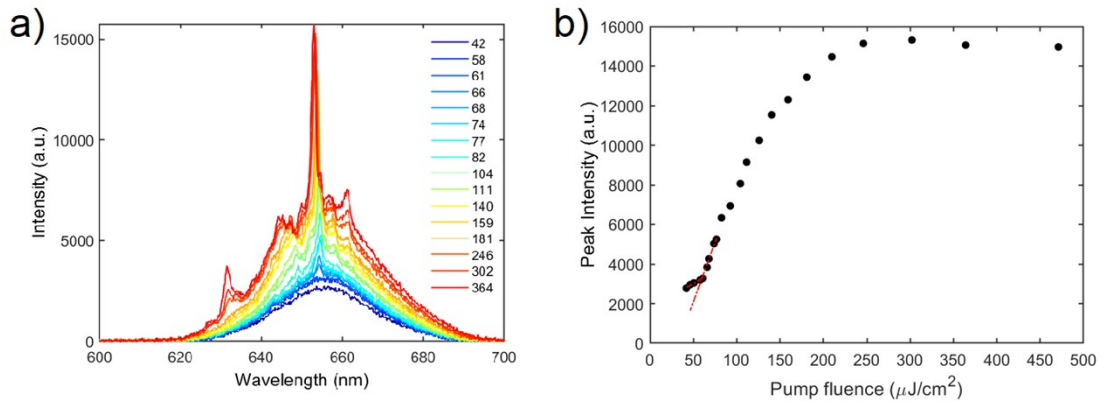

Figure S2. a) Luminescence spectra of the PT-symmetric sample with *f=3.8 %* Ag NPs and b) characteristic light-light graph of the sample.

Full electromagnetic solutions: The optical response of the cavity was modeled using commercially available software (Lumerical FDTD Solutions). Two-dimensional simulations were carried out using perfectly-matched layer (PML) boundary conditions. The model gives us the spatial distribution of the electric field intensity in fiber cross section.

Modal analysis: The modal analyses were carried out using a commercially available software package (Lumerical MODE solution). We performed one-dimensional simulations in radial direction using PML boundary condition. As shown in Figure S3, the bent waveguide analysis was done with the radius of 62.5 μm, to locally model the fiber structure in one dimension. The experimental refractive indices were extracted using ellipsometry measurements.

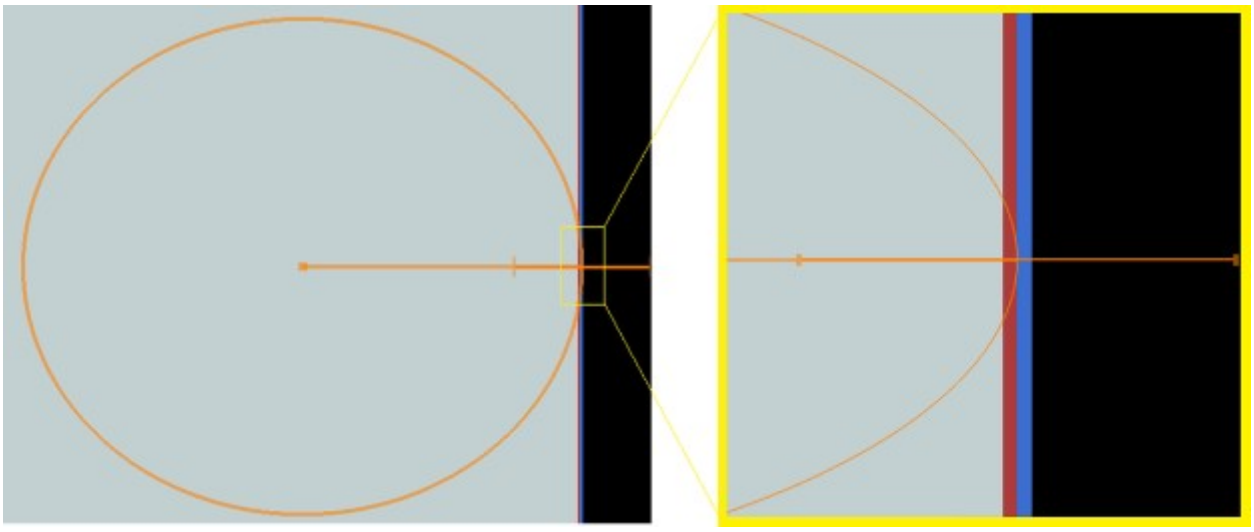

Figure S3. MODE simulation layout. The blue rectangle corresponds to the CQW layer, the red rectangle represents the nanocomposite loss layers, and the gray rectangle is representing the SiO_2 coreless fiber. The orange line shows the 1D simulation region, and the orange circle shows the introduced bent waveguide analysis with the radius of 62.5 μm.

Materials: Cadmium acetate ($Cd(OAc)_2$, 99.995%), sodium myristate (≥99.0%), cadmium acetate dihydrate ($Cd(OAc)_2 \times 2H_2O$, 98%), zinc acetate ($Zn(OAc)_2$, 99.99%), selenium (99.99%), sulfur (99.98%), 1-octanethiol (≥98.5%), oleic acid (OA, 90%), oleylamine (OLA, 70%), 1-octadecene (ODE, 90%), n-hexane (≥97.0%), ethanol (absolute), methanol (≥99.7%) and toluene (≥99.5%) were obtained from Sigma Aldrich, and used with no further change.

Cadmium myristate synthesis: Cadmium myristate powder was synthesized according to the previously published recipe in the literature.[4]

4ML CdSe core CQWs synthesis: 4 ML CdSe core CQWs were synthesized according to the published recipe in the literature with minor modifications.[4] In a typical synthesis, 340 mg of cadmium myristate, 30 mL of ODE and 20 mg of Se were mixed in a 100 mL flask, and degassed at 95 ˚C for one hour. Then, the flask was flushed with argon gas, and the temperature was set to 237 ˚C. At around 190-200 C˚, when the solution becomes golden yellow, 120 mg of $Cd(OAc)_2.2H_2O$ was swiftly added to the flask. The solution remained at 237 ˚C for 7 min, and then 1 mL of OA was added to the flask while quickly after that, the flask was quenched in water. The solution was collected and diluted with 10 mL of hexane, and it was centrifuged at 6000 rpm for 6 min. 4 ML CdSe core CQWs were precipitated from the supernatant by addition of ethanol and centrifugation. The CQWs were redispersed in hexane and kept for further use.

CdSe/CdZnS core/HI shell CQWs synthesis: The CdSe/CdZnS core/HI shell CQWs were synthesized according to the literature with minor modifications.[5] In a typical synthesis, 1 mL of core solution (with optical density of 2 at 350 nm when 200 µL of core solution is diluted in 3 mL of hexane) was taken and precipitated by addition of ethanol and centrifugation. The precipitate was redispersed in hexane and put in a 50 mL flask alongside with 5 mL of ODE, 11.5 mg of $Cd(OAc)_2$, 27.8 mg of $Zn(OAc)_2$ and 0.5 mL of OA. The solution was degassed at room temperature for 1.5 h, and later at 95 C˚ for 30 min. Then the flask was flushed with Ar gas, 0.5 mL of OLA was added to the solution, and the temperature was set to 300 ˚C. At temperature around 165 ˚C, a solution of 1-octanethiol-ODE (0.1 M) was started to be injected into the solution with the rate of 10 mL/h, and at 240 ˚C, the rate of injection was decreased to 4 mL/h. The solution was kept at high temperature of 300 ˚C until 4 mL of the anion precursor was completely injected. Then, the flask was quenched in a water bath, and the solution was collected. 5 mL of hexane was added, and the solution was centrifuged to remove the unstable particles. The supernatant was collected, and the CQWs were separated from the solution and other unwanted species by addition of ethanol and centrifugation. The precipitated CQWs were redispersed in hexane and kept for further use.

Silver nanoparticle (NPs) synthesis: Plasmonic Ag NPs were synthesized according to the previously published report in literature, with minor modifications.[6] In a typical synthesis, 3 g of $AgNO_3$, 75 mL of OLA and 150 mL of ODE were mixed in a 250 mL flask. The solution was degassed at room temperature for 2 h in order to remove the volatile species, especially oxygen. Then, under Ar gas, the temperature was increased to 180 ˚C with heating rate of 8 ˚C/min. The solution was kept at this temperature for 2 h for complete nucleation and growth of the Ag NPs, while the color of the solution was changed from light orange to black at final stages of the growth. Then, in order to focus the size and shape of the NPs, the solution was kept at 150 ˚C for extra 2 h for Ostwald ripening process. At the end, the flask was cooled down to room temperature and diluted with hexane. The solution was collected and centrifuged at 6000 rpm for 5 min to remove the unwanted large NPs. The precipitate was discarded, and Ag NPs were separated from the solution by addition of ethanol and centrifugation. At the end, the precipitated Ag NPs were redispersed in toluene.

Ellipsometry: The complex refractive index of the thin CQW film and PMMA were determined using J.A.Woollam Co., Inc variable angle spectroscopic ellipsometer (VASE) in accordance with previous reports in the literature.[7,8] The changes in ellipsometric Ψ and Δ data were measured at three angles of incidence (55°, 60°, and 65°) from a CQW film deposited on silicon in the 400-800 nm range with 10 nm steps. The thickness of the sample was determined from the spectral region across which the CQWs are non-absorbing (700-800 nm) using a Cauchy model.[9] This thickness was kept fixed and the wavelength range was gradually extended to fit the excitonic features using Kramers-Krönig relation consistent dispersion curves. The complex dielectric function was decomposed into one Tauc-Lorentz oscillator and three Gaussian oscillators. The acquired data analysis was performed using W-Vase32 software package.

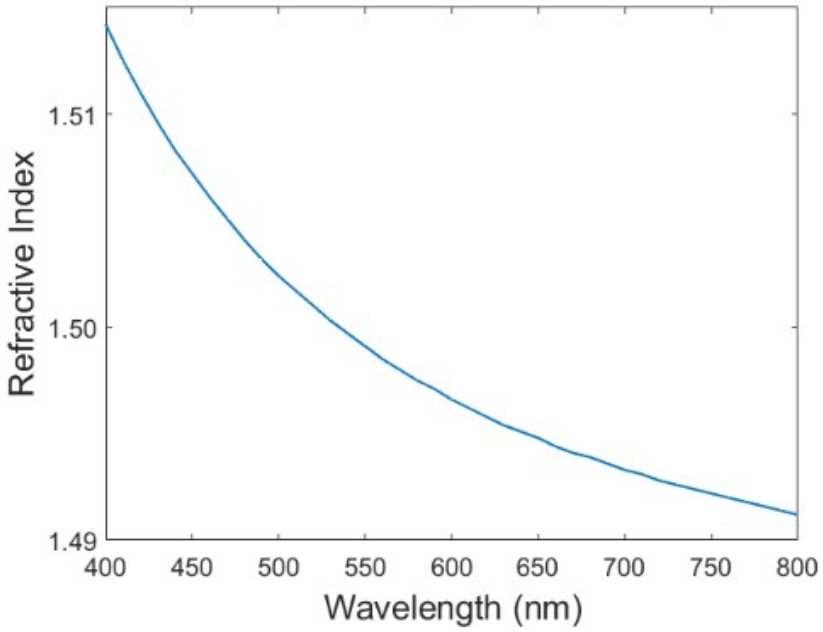

Figure S4. Refractive index of PMMA.

Dip-coating of nanocomposite and CQWs: To form high-density close-packed solid films of CQWs around the coreless fiber, a highly concentrated solution (60–70 mg mL^{-1}) of the CQWs was prepared in hexane. Then, bare fiber was dipped into the solution, thanks to adhesion, after 10–20 min, a thick layer of the CQWs was coated around the fiber. Figure S5 shows the relationship between the thickness and concentration of CQWs.

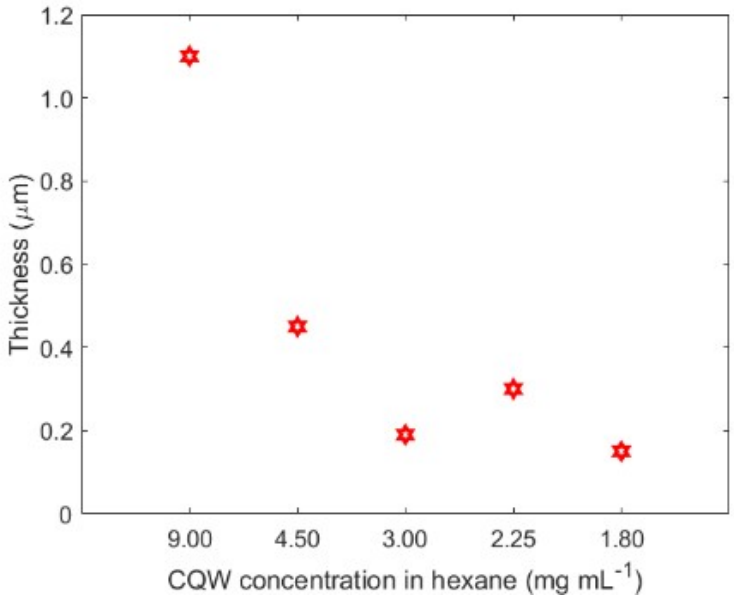

Figure S5. CQW coating thickness as a function of the CQW concentration in solution.

To coat a uniform thick layer of AgNP-PMMA nanocomposite around the coreless fiber, the lifting speed of fiber from nanocomposite was controlled.

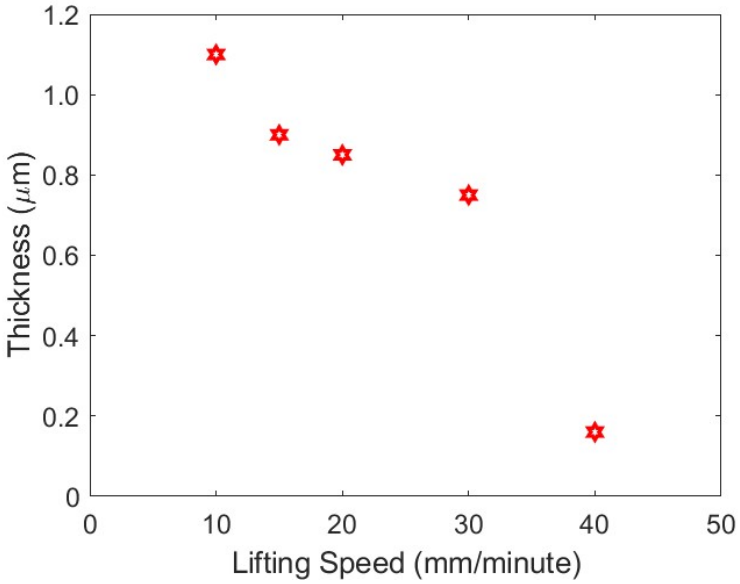

Figure S6. Nanocomposite coating thickness as a function of the lifting speed.

Lasing measurement: As the pump excitation, we used a femtosecond mode-locked Ti:sapphire amplifier (Spectra Physics, Spitfire Pro) with a 1 kHz repetition rate and a 120 fs pulse width, operating at 800 nm wavelength, which is frequency-doubled with a BBO crystal at the output to 400 nm. The pump fluence on the sample was changed using a variable neutral density filter. A spherical lens with a 3 cm focal length

was used to focus the excitation onto the fiber. The PL signal was collected with the help of an optical fiber connected to a PL spectrometer (Avantes, AVASPEC-ULS3648TEC).

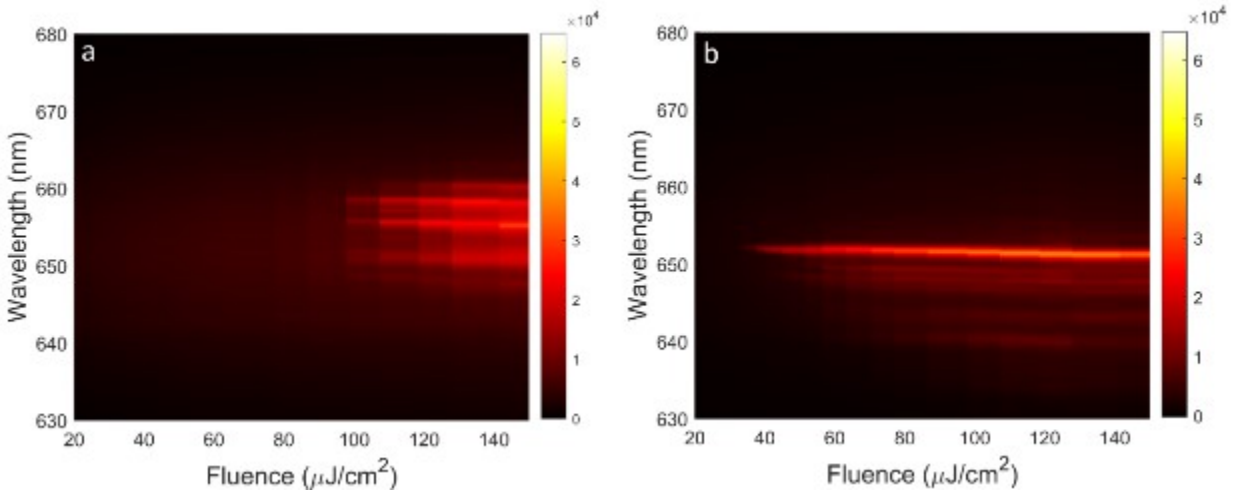

Figure S7. Measured lasing spectra at various pumping energy densities. a) Control sample and b) PT-symmetric sample.

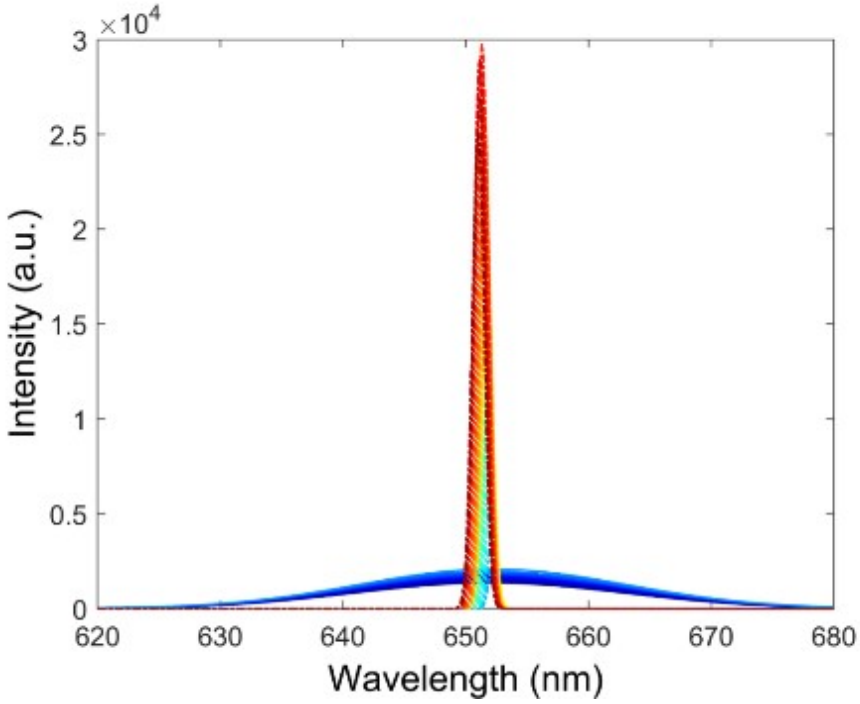

Figure S8. Gaussian fits for the measured lasing spectra of PT-symmetric sample.

References

1 L. Feng, Z. J. Wong, R. M. Ma, Y. Wang and X. Zhang, *Science*, 2014, **346**, 972–975.

2 Q. Zeng, E. Lafalce, C. H. Lin, M. J. Smith, J. Jung, Y. Yoon, Z. Lin, V. V. Tsukruk and Z. V.

Vardeny, *Nano Lett.*, 2019, **19**, 6049–6057.

3 O. Erdem, S. Foroutan, N. Gheshlaghi, B. Guzelturk, Y. Altintas and H. V. Demir, *Nano Lett.*, 2020, **20**, 9, 6459–6465.

4 E. Ebrahimi, M. Irfan, F. Shabani, Y. Kocak, B. Karakurt, E. Erdem, H. V. Demir and E. Ozensoy, *ChemCatChem*, 2020, **12**, 6329–6343.

5 N. Gheshlaghi, S. Foroutan-Barenji, O. Erdem, Y. Altintas, F. Shabani, M. H. Humayun and H. V. Demir, *Nano Lett.*, 2021, **21**, 4598–4605.

6 M. Chen, Y. G. Feng, X. Wang, T. C. Li, J. Y. Zhang and D. J. Qian, *Langmuir*, 2007, **23**, 5296–5304.

7 B. T. Diroll, E. A. Gaulding, C. R. Kagan and C. B. Murray, *Chem. Mater.*, 2015, **27**, 6463–6469.

8 D. B. Dement, M. Puri and V. E. Ferry, *J. Phys. Chem. C*, 2018, **122**, 21557–21568.

9 W. A. McGahan, B. Johs and J. A. Woollam, *Thin Solid Films*, 1993, **234**, 443–446.